NANO LETTERS
Letter
pubs.acs.org/NanoLett

Disorder Imposed Limits of Mono- and Bilayer Graphene Electronic Modification Using Covalent Chemistry

Chih-Jen Shih,[†] Qing Hua Wang,[†] Zhong Jin,[†] Geraldine L. C. Paulus,[†] Daniel Blankschtein,[†] Pablo Jarillo-Herrero,[‡] and Michael S. Strano*,[†]

[†]Department of Chemical Engineering and [‡]Department of Physics, Massachusetts Institute of Technology, Cambridge, Massachusetts 02139, United States

Supporting Information

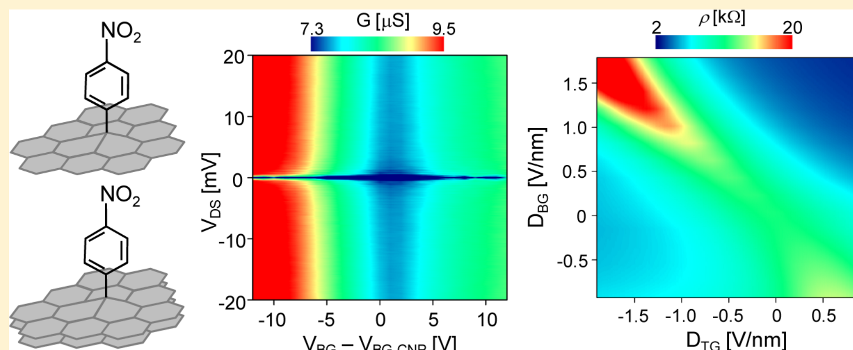

ABSTRACT: A central question in graphene chemistry is to what extent chemical modification can control an electronically accessible band gap in monolayer and bilayer graphene (MLG and BLG). Density functional theory predicts gaps in covalently functionalized graphene as high as 2 eV, while this approach neglects the fact that lattice symmetry breaking occurs over only a prescribed radius of nanometer dimension, which we label the S-region. Therefore, high chemical conversion is central to observing this band gap in transport. We use an electrochemical approach involving phenyl-diazonium salts to systematically probe electronic modification in MLG and BLG with increasing functionalization for the first time, obtaining the highest conversion values to date. We find that both MLG and BLG retain their relatively high conductivity after functionalization even at high conversion, as mobility losses are offset by increases in carrier concentration. For MLG, we find that band gap opening as measured during transport is linearly increased with respect to the I_D/I_G ratio but remains below 0.1 meV in magnitude for SiO_2 supported graphene. The largest transport band gap obtained in a suspended, highly functionalized (I_D/I_G = 4.5) graphene is about 1 meV, lower than our theoretical predictions considering the quantum interference effect between two neighboring S-regions and attributed to its population with midgap states. On the other hand, heavily functionalized BLG (I_D/I_G = 1.8) still retains its signature dual-gated band gap opening due to electric-field symmetry breaking. We find a notable asymmetric deflection of the charge neutrality point (CNP) under positive bias which increases the apparent on/off current ratio by 50%, suggesting that synergy between symmetry breaking, disorder, and quantum interference may allow the observation of new transistor phenomena. These important observations set definitive limits on the extent to which chemical modification can control graphene electronically.

KEYWORDS: *Graphene, bilayer graphene, transport band gap, chemical functionalization, disorder*

Graphene, with atomic sheets consisting of fewer than 10 stacked layers of sp^2-hybridized carbon lattice,[1] has emerged as a promising candidate material for postsilicon nanoelectronics due to its ultrahigh carrier mobility.[2−4] Recent progress in tuning the band gap and resistivity in AB-stacked bilayer graphene by breaking the symmetry between the top and bottom graphene planes[5−12] has shed further light on engineering the transport properties of graphene. Nevertheless, for most potential applications, these materials require advanced methods to open a more significant transport band gap without sacrificing their intrinsic mobilities. To enable semiconducting behavior in graphene, various physical approaches have been proposed, including nanoribbons,[13−15] nanomeshes,[16] and strain engineering.[17,18] However, these approaches generally involve ultraprecise processing, which remains a significant challenge for mass production.

Several theoretical and empirical studies of covalent graphene chemistry[19−24] predict its ability to open a controllable band gap in monolayer graphene (MLG) and bilayer graphene (BLG), a longstanding goal of the field. Methods of functionalizing graphene have advanced considerably in recent

Received: December 15, 2012
Revised: January 18, 2013
Published: January 22, 2013

© 2013 American Chemical Society

years. Numerous chemical routes, including hydrogenation,[20,21,25] oxidation,[26−28] fluorination,[22,29−31] and aryl diazonium chemistry,[32−39] have been developed. Among these methods, covalent functionalization using aryl diazonium salts occurs by an electron transfer mechanism, where a delocalized electron is transferred from the graphene lattice to an adjacent reactant, forming a radical, which then forms a covalent bond with a graphene carbon atom and therefore grafts onto its surface. The electron transfer chemistry of graphene is directly influenced by the localized fluctuation of Fermi level due to electron−hole puddles induced by charged impurities in the substrate,[40,41] as well as by the edge disorders.[34,36] Due to these extrinsic effects, to date, the chemical routes used lack an ability to control the reaction rate in a uniform and efficient manner, particularly for multilayer (>1) graphene.[20,33,36]

On the other hand, after covalent functionalization, the sp^2 lattice is partially distorted and interspersed with sp^3 regions.[42] Theoretically, there are two mechanisms underlying the formation of a band gap in covalently functionalized MLG: (i) a large band gap (∼1−2 eV)[19] created around the structurally disordered region (the S-region)[43] due to the sp^3 hybridization, and (ii) a relatively small band gap (∼100 meV) created in the pristine sp^2 lattice between two neighboring S-regions due to the quantum interference phenomena.[42] Experimentally, an optical band gap up to hundreds of meV has been observed.[33] However, despite this activity, the engineering of such a gap of such magnitude under electronic transport conditions has not been realized. The transport characteristics of functionalized graphene devices often exhibit a strong suppression of carrier mobility, and the resulting transport band gap is either ambiguous or not consistent with the optical band gap.[21,31,35,37,38] There remains a lack of fundamental understanding of electronic transport in functionalized graphene, including its dependence on the degree of functionalization. Moreover, to the best of our knowledge, the electronic characteristics of covalently functionalized bilayer graphene have never been investigated.

In this report, we develop an efficient method to functionalize graphene using an electrochemical aryl diazonium chemistry to achieve the highest levels of lattice conversion to date for MLG and BLG. We study the transport characteristics of bottom-gated monolayer and dual-gated bilayer graphene field effect transistors (FETs) and measure the transport band gap opened precisely as a function of the degree of chemical functionalization. Accordingly, this work establishes the experimental limits of graphene chemistry for controlling its electronic structure.

Results and Discussion. *Electrochemical Aryl Diazonium Chemistry.* MLG and BLG FET devices were fabricated using the micromechanical cleavage process[1] to isolate graphene flakes on 300 and 100 nm SiO_2/p-doped Si substrates, respectively. The source and drain contacts were patterned onto the flakes utilizing photolithography, followed by the deposition of Ti/Au contact electrodes. The detailed fabrication process is described in Supplementary Section S1. The transport properties of the pristine MLG and BLG devices were characterized at 14 K. The typical mobility is 8000−16 000 $cm^2/(V\ s)$ and 1000−3000 $cm^2/(V\ s)$ for MLG and BLG devices, respectively. These devices were subsequently functionalized, as shown schematically in Figure 1a. Specifically, an electrochemical functionalization was carried out in an acetonitrile solution with 20 mM nitrobenzene diazonium (4-nitrobenzene diazonium tetrafluoroborate) or bromobenzene

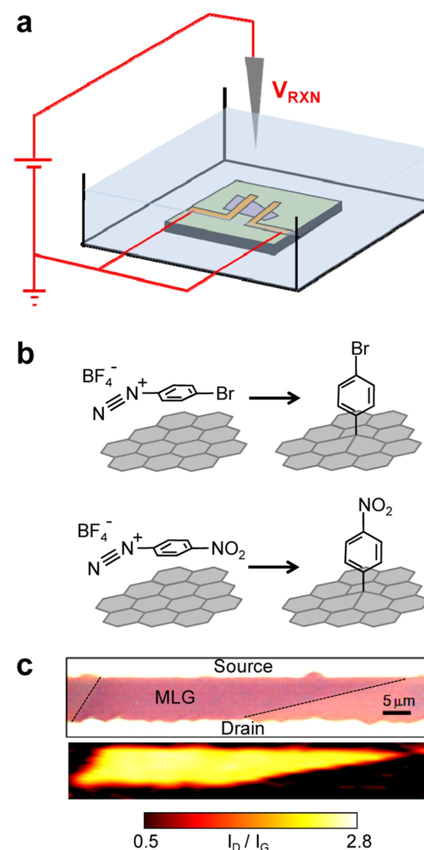

Figure 1. (a) Schematic diagram of the electrochemical aryl diazonium chemistry on a graphene FET device. (b) Schematic of the electron transfer chemistry between graphene and 4-bromobenzene diazonium tetrafluoroborate (top) and 4-nitrobenzene diazonium tetrafluoroborate (bottom) to form covalently functionalized graphene grafted with bromophenyl (Br-ph) and nitrophenyl (NO_2-ph) groups, respectively. (c) Optical microscope image (top) and Raman map of the I_D/I_G (bottom) of a functionalized MLG device using V_{RXN} = 1 V and grounded source and drain electrodes.

diazonium (4-bromobenzene diazonium tetrafluoroborate). The source and drain electrodes were electrically grounded, and a positive voltage V_{RXN} was applied to the solution using a tungsten probe for 30 s. Consequently, aryl diazonium groups were grafted onto graphene surfaces through electron transfer reaction to form bromophenyl (Br-ph) or nitrophenyl (NO_2-ph) functionalized graphene, as shown in Figure 1b. The applied electric field creates an electrical double layer adjacent to the graphene surface,[44] such that the Fermi level of graphene is raised, thereby increasing the rate of electron transfer reaction.[45] Note that the increase in Fermi level in this experiment greatly exceeds the typical value of electron−hole puddle amplitudes in graphene on SiO_2, allowing us to neglect the substrate effect observed previously.[28] The positive V_{RXN} also concentrates the diazonium cations (see Figure 1b) within the double layer to accelerate the reaction. More importantly, because of a more precise control of the Fermi-level position, the reaction rate is expected to be more spatially uniform than that using conventional electron transfer chemistries, although Hersam and Wang[46] have demonstrated that multiaromatic oligomers form on the graphene surface at high chemical conversion, as seen for graphite electrodes as well.[46] Because in this work we are concerned only with symmetry breaking lattice defects, correlating them with the extent of band gap opening,

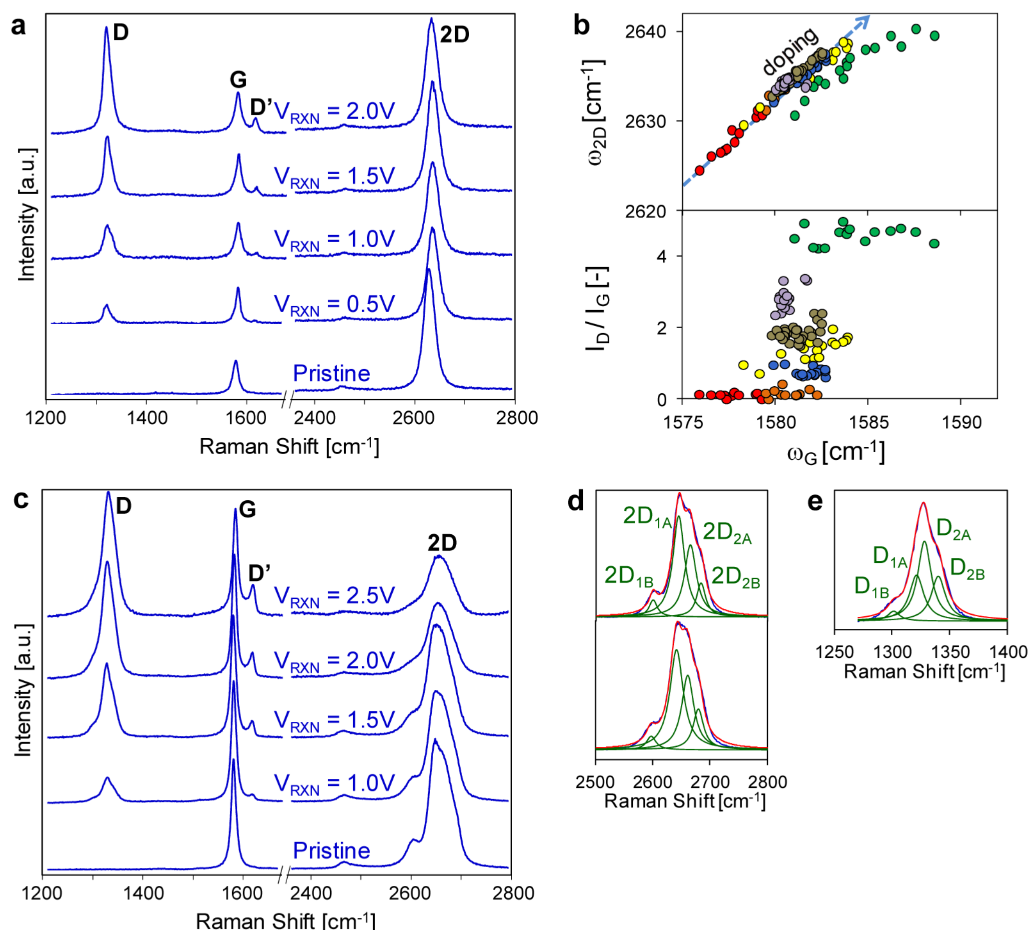

Figure 2. Representative Raman spectra (with λ_{EX} = 633 nm) of NO_2-ph functionalized (a) MLG and (c) BLG using different values of V_{RXN}. (b) $2D$ peak position (ω_{2D}, top) and I_D/I_G (bottom) for functionalized MLG as a function of G peak position (ω_G), with doping trajectory adapted from refs 44 and 45. Spectra taken from different samples using different V_{RXN} are presented using different colors. (d) The $2D$ peaks of a pristine (top) and functionalized (bottom) BLG and the fits of four Lorentzian components. (e) The D peak of a functionalized BLG and the fit of four Lorentzian components.

we ignore oligomer formation because it can only reduce the maximum possible chemical conversion. Before characterization, each graphene device was rinsed with copious amounts of acetonitrile to minimize residual physisorption of diazonium molecules.[47] Figure 1c shows a representative functionalized MLG device using V_{RXN} = 1 V. Its Raman image of the integrated intensity ratio of the D to G peaks (I_D/I_G) is also shown. It is noteworthy that unlike conventional aryl diazonium chemistry, we did not observe a significantly higher degree of functionalization at the edge of graphene,[34,36] implying that the Fermi level increase due to the electric field applied to the solution overwhelms the effect of the edge disorder.

Representative Raman spectra corresponding to various values of V_{RXN} for MLG and BLG are shown in Figure 2a and c, respectively. The spectrum of pristine MLG has two prominent peaks, the G and $2D$ peaks, located around 1580 cm^{-1} and 2630 cm^{-1}, respectively.[48] After diazonium functionalization, stronger D (~ 1315 cm^{-1}) and D' (~ 1615 cm^{-1}) peaks become apparent due to the formation of sp^3 hybridization[33] using a higher value of V_{RXN}. For each spectrum, each of the four peaks can be well fitted with single Lorentzians.[33] The peak parameters from fitting the peaks to Lorentzian functions were extracted, and the scatter plots for the $2D$ peak position (ω_{2D}) and I_D/I_G as a function of the G peak position (ω_G) are shown in Figure 2b. The dashed line corresponds to the trajectory of increasing n- or p-doping in pristine graphene, which leads to an increase of ω_G.[45,46] Interestingly, both pristine and functionalized graphene follow the doping trajectory except the most functionalized ones (see Figure 2b top). In addition, since ω_G does not increase significantly with I_D/I_G, it suggests that covalent functionalization itself does not increase the level of doping (see Figure 2b bottom). The slight upshift of ω_G in functionalized graphene can be attributed to the physisorption of diazonium cation and oligomers.[47]

Using the electrochemical aryl diazonium reaction, BLG can be functionalized to a significantly high degree, as shown in Figure 2c. The D, G, D', and $2D$ peaks of pristine and functionalized BLG can be found around 1320, 1580, 1615, and 2640 cm^{-1}, respectively. This level of functionalization for BLG is unprecedented in the literature to date. For the first time, we observe that the D (Figure 2e) and $2D$ peaks of pristine (Figure 2d top) and covalently functionalized (Figure 2d bottom) BLG are all asymmetric and can be decomposed into four Lorentzians, similar to previous reports of ion bombardment defects in bilayer graphene.[49] The four components of the $2D$ peak ($2D_{1B}$, $2D_{1A}$, $2D_{2A}$, and $2D_{2B}$, see Figure 2c) result from the splitting of the phonon branches in BLG.[48,50] The covalent functionalization, which presumably introduces defects in the

dx.doi.org/10.1021/nl304632e | Nano Lett. 2013, 13, 809−817

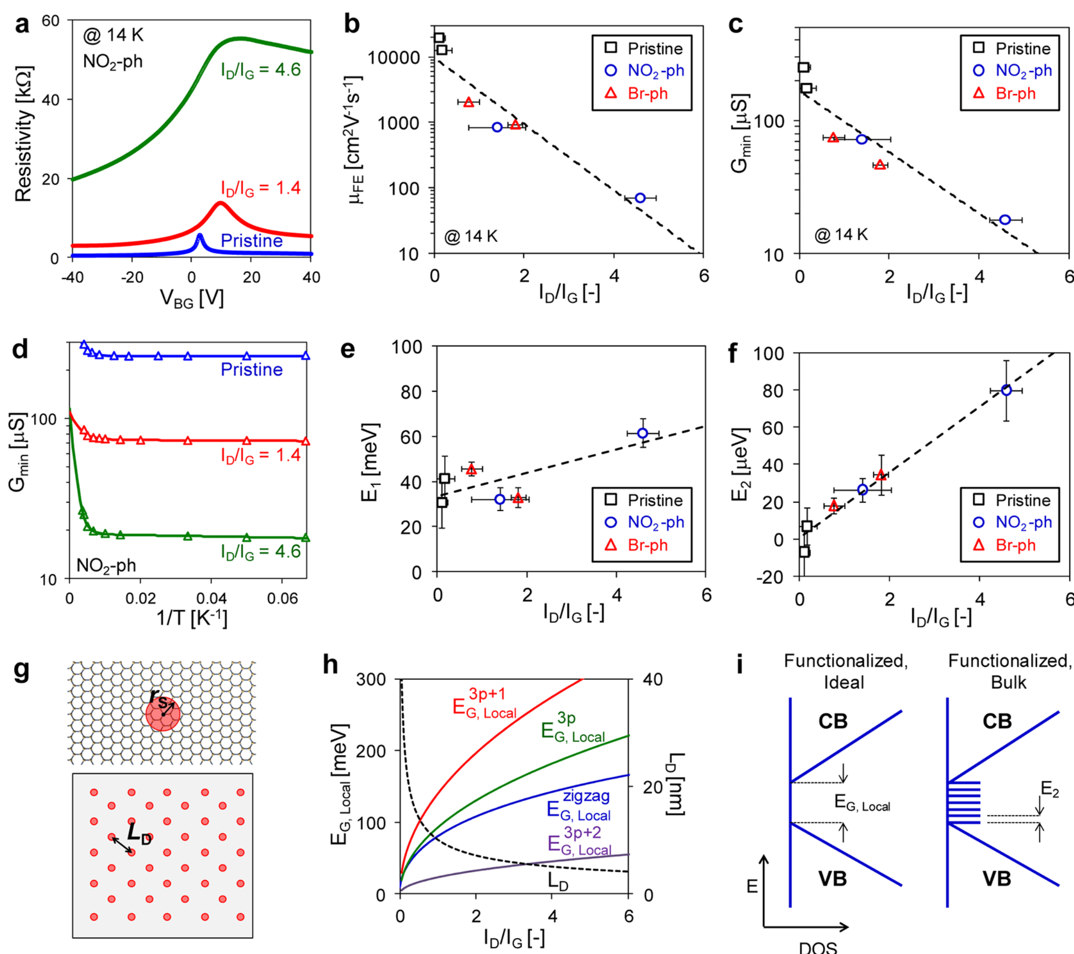

Figure 3. Transport characteristics of functionalized MLG. (a) Resistivity vs V_{BG} curves for a pristine MLG device, an MLG device characterized by I_D/I_G = 1.4 and one with I_D/I_G = 4.6. Extracted values of (b) μ_{FE} and (c) G_{min} as a function of I_D/I_G. (d) G_{min} as a function of inverse temperature from 14 to 200 K for three MLG devices. Extracted values of (e) E_1 and (f) E_2 as a function of I_D/I_G using eq 4. (g) Schematics of the structurally disordered region (S-region, top) around a grafted functional group and the sheet of functionalized MLG (bottom). (h) Calculated $E_{G,Local}$ and L_D as a function of I_D/I_G using eqs 2–6. (i) Schematics of the proposed band structures for functionalized MLG (CB: conduction band; VB: valence band).

top graphitic layer only (the layer in contact with the solution during reaction) in BLG, reduces the relative intensities of $2D_{1B}$ and $2D_{1A}$, suggesting a different degree of change in the exchange phonon momentum between the two phonon branches during the second-order double resonance (DR) process.[48] On the other hand, since the associated first-order DR process of BLG is activated by the formation of sp^3 hybridization,[48] it is reasonable that the *D* peak of BLG shares the same spectroscopic features as the 2*D* peak, as shown in Figure 2e. More detailed research to understand the phonon behavior in functionalized BLG using Raman spectroscopy is underway and will be published in a subsequent report.

For comparison, the same electron transfer chemistry in the absence of external electrochemical bias is capable of functionalizing MLG to $I_D/I_G \sim 2$, which corresponds to V_{RXN} of approximately 1.5 V in our method (see Figure 2a), but is unable to functionalize BLG to an observable degree as we have previously reported.[33,34,36] However, the method developed in this work can readily functionalize BLG with $V_{RXN} \geq 1$ V, and the difference in reactivity between MLG and BLG is significantly diminished compared those reported.[20,33,36] In this study, the highest degree of functionalization with $I_D/I_G \sim 2$ is achieved using V_{RXN} = 2.5 V. This is consistent with the previous observation that the reaction rate in an unbiased electron transfer reaction[20,33,36] of MLG is dominated by the localized fluctuation of Fermi level caused by the underlying substrate,[40] which is suppressed in BLG due to screening from an additional graphitic layer.[34,51] Using our method, since we functionalize graphene by raising its Fermi level directly, the difference in reactivity between MLG and BLG is mainly determined by the relatively small difference of density of states (DOS) around the Dirac point.[51] Note that it is expected that I_D/I_G for BLG is approximately half of that for MLG, since the former, as we observe, has an inaccessible graphene layer.

Electronic Transport in Functionalized MLG. To study the effect of chemical functionalization on the electronic transport in graphene, FET devices with various degrees of functionalization were prepared using the aforementioned method. Before electronic characterization, 20 Raman spectra were taken randomly in each sample to obtain an average I_D/I_G value. All devices were characterized at 14 K. The resistivity of MLG between the source and drain electrodes as a function of bottom gate (BG) voltage, V_{BG}, for a pristine device, one with I_D/I_G = 1.4, and one with I_D/I_G = 4.6, are shown in Figure 3a. Each curve exhibits a clear maximum resistivity, R_{max}, which

occurs where the Fermi level coincides with the Dirac point (the so-called charge neutrality point (CNP)), and the corresponding V_{BG} is $V_{BG,CNP}$. In bottom-gated devices, the parallel-plate capacitor model yields a field-effect charge density $n_{FE} = C_{BG}(V_{BG} - V_{BG,CNP})$, where C_{BG} is the bottom-gate capacitance. Comparing to the pristine, unfunctionalized device, the functionalization introduces a positive shift in $V_{BG,CNP}$, which corresponds to additional 5.21×10^{11} (I_D/I_G = 1.4) and 9.34×10^{11} cm^{-2} (I_D/I_G = 4.6) holes doped to the MLG devices. The p-type doping also hinders the electron conduction, which is associated with $V_{BG} > V_{BG,CNP}$,[47] such that electron−hole conduction asymmetry was observed in the samples with high I_D/I_G.

The calculated field-effect hole mobilities, μ_{FE}, and the minimum conductivities, $G_{min} = 1/R_{max}$, for several MLG devices as a function of the measured I_D/I_G values are shown in Figure 3b and c, respectively. Despite the fact that μ_{FE} and G_{min} decrease exponentially with I_D/I_G, the reduction rate of μ_{FE} is found to be anomalously 100 times higher than that of G_{min}.

The counterbalancing influences of scattering and doping, both of which are changed after chemical functionalization, are predicted in even a classical depiction of carrier transport. For example, the electronic conductivity in a solid can be described by the Drude-Lorentz model:[52]

$$G = \frac{ne^2\Lambda}{m^* v_F} \tag{1}$$

where G is the conductivity, n is the total charge density, e is the elementary charge, m^* is the effective mass of carriers, Λ is the mean free path of carriers, and v_F is the Fermi velocity. The mobility of carriers, μ, in a typical semiconductor is given by:[52]

$$\mu = \frac{e\Lambda}{m^* v_F} = \frac{G}{ne} \tag{2}$$

In the specific case for the total charge density in MLG, n can be expressed as:

$$n = n_{FE} + n_i \tag{3}$$

where n_i is the charge density resulting from the formation of electron−hole puddles in graphene due to the charged impurities.[53] While μ_{FE} and G_{min} are compared at different charge densities in this work (and charge carriers in MLG mimic relativistic particles with zero mass in contrast to eq 2), eqs 1−3, illustrate the counterbalance between scattering and carrier doping. Specifically, the strong reduction of mobility with I_D/I_G implies that the structural defects generated during the functionalization process significantly reduce the mean free path from ∼100 nm (pristine, $\mu_{FE} \sim 10\,000$ cm^2/(V s)) to ∼1 nm ($I_D/I_G = 6$, $\mu_{FE} \sim 10$ cm^2/(V s)). However, since G_{min} only weakly decreases with I_D/I_G, it appears that the charge density, n, in eq 1 increases significantly. At the CNP, where G_{min} is characterized, the electronic transport is dominated by the formation of electron−hole puddles, n_i, because $n_{FE} = 0$.[53] This evidence clearly suggests that additional charge impurities, n_i, are introduced due to chemical functionalization.

To obtain additional insight into the electronic band structure of functionalized MLG, we studied the temperature dependence of G_{min} in the range of 14−200 K. Figure 3d shows the measured G_{min} as a function of inverse temperature, $1/T$, for three different values of I_D/I_G. We observe two distinct temperature regimes: a fast decrease of the conductivity from 200 to 100 K, followed by a much weaker temperature dependence from 100 to 14 K. For the temperatures considered, we found that the conductivity can be well-described by an activation model with two different activation energies:

$$G_{min} = G_1 \exp\left(\frac{-E_1}{k_B T}\right) + G_2 \exp\left(\frac{-E_2}{k_B T}\right) \tag{4}$$

where G is the conductivity, E is the activation energy, k_B is the Boltzmann constant, and the subscripts 1 and 2 correspond to the regimes of strong and weak temperature dependence, respectively. The temperature-dependent behavior was also observed in dual-gated BLG devices.[10,11] The extracted activation energies, E_1 and E_2, are plotted versus the corresponding I_D/I_G in Figure 3e and f, respectively. The higher energy, E_1, corresponds to thermal excitation of carriers across the Dirac point,[4] and only exhibits a weak dependence on I_D/I_G. The temperature dependence in the high-temperature regime is not originated from the formation of band gap and has often been observed in high-quality graphene samples.[4] On the other hand, the low energy, E_2, exhibits a linear dependence on I_D/I_G and is therefore possibly proportional to the effective transport band gap.[10,11] Note that the weak temperature dependence of G_{min} in the low-temperature regime does not necessarily suggest the formation of transport band gap since the extracted values of E_2 are considerably smaller than k_BT. Other transport mechanisms (e.g., variable range hopping)[35] may also play an important role.

After covalent functionalization, the sp^2 lattice is partially distorted and interspersed with sp^3 regions (a schematic diagram of a functionalized MLG is shown in Figure 3g). Theoretically, there are two mechanisms underlying the formation of a band gap in covalently functionalized MLG: (i) a large band gap (∼1−2 eV predicted by DFT calculations)[19] created around the structurally disordered region (S-region, see Figure 3g top)[43] due to the sp^3 hybridization, and (ii) a relatively small band gap (∼100 meV) created in the pristine sp^2 lattice between two neighboring S-regions due to the quantum interference phenomena (see Figure 3g bottom). Based on the schematic shown in Figure 3g, we propose a model to estimate the transport band gap created in functionalized graphene. First, the experimentally measured I_D/I_G is empirically given by:[43]

$$\frac{I_D}{I_G} = \frac{102}{{L_D}^2} \tag{5}$$

where L_D is the average distance (in units of nm) between the centers of the S-regions (see Figure 3g bottom). Equation. 5 suggests that $L_D > 4$ nm for the degree of functionalization considered here. Since this value is much larger than the radius of the S-region, r_S (∼ 0.5 nm),[41] it appears that the creation of a band gap in functionalized graphene is dominated by the quantum interference effect, and the sp^2 lattice of graphene is mostly preserved after functionalization. Note that eq 5 was estimated in physically defective graphitic materials,[43] while recent findings in covalently functionalized graphene suggest that the value of L_D may be smaller than 1 nm.[32,33] To model the electronic transport through the "channels" between the S-regions, the following assumptions were made: (i) the S-region is electrically insulating; (ii) the radius of the S-region, r_s, is much smaller than L_D; and (iii) the edges of a conducting channel between two S-regions can be modeled approximately as either hydrogen-passivated armchair or zigzag conforma-

dx.doi.org/10.1021/nl304632e | Nano Lett. 2013, 13, 809−817

tions. Therefore, the local electronic transport in covalently functionalized MLG is analogous to that in a graphene nanoribbon (GNR)[13] of width L_D. The local band gaps, $E_{G,Local}$, corresponding to the armchair edges with dimer lines $N_a = 3p$, $3p + 1$, and $3p + 2$, where p is an integer, are given by:[13]

$$E_{G,Local}^{3p} = \Delta_{3p}^{0} - \frac{8t\delta}{3p+1}\sin^2\left(\frac{p\pi}{3p+1}\right) \tag{6}$$

$$E_{G,Local}^{3p+1} = \Delta_{3p+1}^{0} + \frac{8t\delta}{3p+2}\sin^2\left[\frac{(p+1)\pi}{3p+2}\right] \tag{7}$$

$$E_{G,Local}^{3p+2} = \frac{2t\delta}{p+1} \tag{8}$$

where $\Delta_{3p}^{0} = t[4\cos(p\pi/(3p+1)) - 2]$, $\Delta_{3p+1}^{0} = t[2 - 4\cos(((p+1)\pi)/(3p+2))]$, $t = 2.7$ eV, and $\delta = 0.12$.[13] The channel width $L_D = 3^{1/2}(N_a - 1)a/2$, where $a = 1.42$ Å is the lattice parameter. The $E_{G,Local}$ of zigzag edges is given by:[13]

$$E_{G,Local}^{zigzag} = \frac{9.33}{L_D + 15} \tag{9}$$

Figure 3h shows the calculated $E_{G,Local}$ and L_D as a function of I_D/I_G using eqs 5−9. The present model predicts the formation of a 50−300 meV local band gap in highly functionalized MLG ($I_D/I_G \sim 5$), which is approximately 3 orders of magnitude larger than the effective transport band gap, E_2 (see Figure 3f).

The findings support the influence of disorder.[10,11] In pristine MLG, charges and impurities have been proposed to be the dominant sources of scattering.[53,54] The impurities affect the electric potential experienced and result in the formation of electron−hole puddles[53] and localized trap states near the Dirac point.[55] The density of states near the Dirac point in bulk MLG is therefore increased. In functionalized MLG, as shown in Figure 3i, although ideally a local band gap, $E_{G,Local}$, is created due to the quantum interference effect, a significant amount of disorder, including impurities and the grafted functional groups, is induced on the graphene surface during functionalization, such that numerous midgap states are generated.[55] Moreover, considering the effects of a spatially inhomogeneous distribution of L_D and Fermi level, it is not surprising that the effective transport band gap, E_2, in bulk MLG is greatly reduced. Since the formation of midgap states also introduces additional charges near the Dirac point, it also explains why the obtained G_{min} only decreases weakly with I_D/I_G. Hence, it is not strictly appropriate to apply the activated model in eq 4 for E_2 values that are exceedingly small as measured in this work. In this case, the interpretation is instead that of an effective activation barrier compromised via disorder induced midgap states, analogous to an effective activation energy in chemical kinetics. In the limit as the purity of graphene and its environment increase, this effective barrier converges to the transport band gap.

Measurements of the conductivity, G, of a highly functionalized MLG device ($I_D/I_G = 4.6$) as a function of drain-source voltage, V_{DS}, and ($V_{BG} - V_{BG,CNP}$) are shown in Figure 4a. At the CNP ($V_{BG} - V_{BG,CNP} = 0$), we did not observe any V_{DS}-dependent behavior. Hence, the transport band gap is not detectable, since the effective transport gap (see Figure 3f) is much smaller than the value of k_BT at 14 K. To further elucidate the role of disorder in electronic transport, the functionalized MLG device was suspended using the method

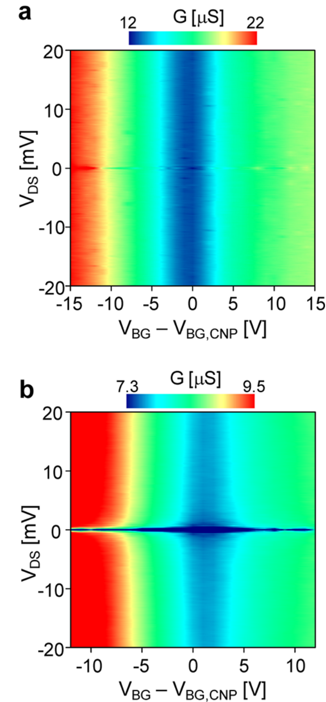

Figure 4. Measured conductivities as a function of V_{DS} and ($V_{BG} - V_{BG,CNP}$) for a highly functionalized MLG device ($I_D/I_G = 4.6$) (a) before and (b) after suspension.

proposed by Bolotin et al.[3] Briefly, the device on SiO_2 was immersed in 7:1 buffered oxide etch for 90 s, which etches away approximately 50% of the SiO_2, including the area under the graphene.[3] Figure 4b shows the obtained values of G as a function of V_{DS} and ($V_{BG} - V_{BG,CNP}$). The conductivity of the functionalized MLG was approximately reduced by half, and a clear V_{DS}-dependent regime is present near the CNP. The onset of V_{DS}-dependence occurs around $V_{DS} = \pm 1$ mV, indicating a ∼1 meV transport gap formed in the suspended sample. This value is about 1 order of magnitude higher than that in the unsuspended device. Although the disorder induced during chemical functionalization still exists, the suspension process reduces the effect of electron−hole puddles from the substrate. This finding further confirms that the electronic transport in functionalized MLG is greatly influenced by this disorder.

Electronic Transport in Functionalized BLG. Next, we investigated if covalent functionalization could increase the electronic band gap formed by utilizing a transverse electric field in BLG.[5−12] Dual-gated devices were fabricated by growing a thin layer of Al_2O_3 at low temperature (50 °C) on functionalized BLG using atomic layer deposition. The top gate (TG) electrode was then patterned onto the device utilizing photolithography, followed by the deposition of the Ti/Ag electrode. A schematic diagram and microscope image of a representative BLG device are shown in Figure 5a. The detailed fabrication process is described in Supplementary Section S2. All of the devices were characterized at 14 K. Figure 5b shows the resistivity of a pristine BLG as a function of top-gate voltage, V_{TG}, using various values of V_{BG}. For each curve, similar to the bottom-gated devices, the maximum resistivity, R_{max}, is associated with the CNP, where the field-effect charge density $n_{FE} = C_{BG}(V_{BG} - V_{BG}^{D}) + C_{TG}(V_{TG} - V_{TG}^{D}) = 0$. C_{TG} is the top-gate capacitance, and (V_{BG}^{D},V_{TG}^{D}) are the bottom- and

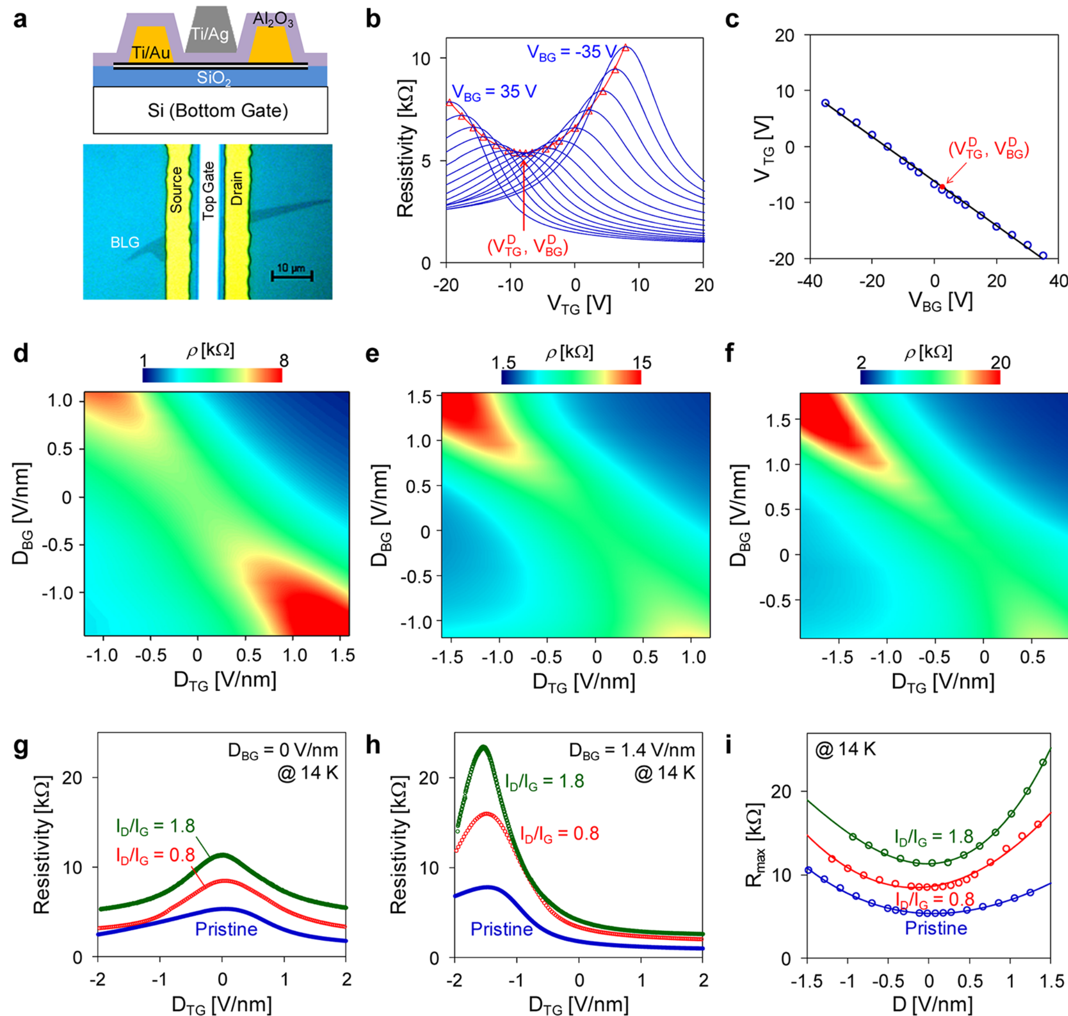

Figure 5. Transport characteristics of NO_2-ph functionalized BLG. (a) Schematic diagram (top) and microscope image (bottom) of a dual-gated BLG device. (b) Resistivity vs V_{TG} curves at various values of V_{BG}. (c) The linear relation between V_{TG} and V_{BG} at various CNPs. Measured resistivities as a function of D_{BG} and D_{TG} for (d) pristine, (e) $I_D/I_G = 0.8$, and (f) $I_D/I_G = 1.8$ BLG devices. Resistivity vs D_{TG} curves for the three BLG devices considered under (g) $D_{BG} = 0$ V/nm and (h) $D_{BG} = 1.4$ V/nm. (i) R_{max} as a function of D for the three BLG devices considered.

top-gate voltages at a specific CNP, where the value of R_{max} reaches its minimum for a standard BLG device.[8] Figure 5c shows the measured values of V_{BG} and V_{TG} of a BLG device at various CNPs. Note that V_{BG} and V_{TG} are linearly related with a slope of $-(C_{BG}/C_{TG})$.[8] To normalize the top- and bottom-gate electric fields, following the convention proposed by Zhang et al.,[8] we define the bottom-gated and top-gated electric displacement fields using $D_{BG} = \varepsilon_{BG}(V_{BG} - V_{BG}^{D})/d_{BG}$ and $D_{TG} = \varepsilon_{TG}(V_{TG} - V_{TG}^{D})/d_{TG}$, where ε is the permittivity and d is the thickness of gate dielectric. The average electric displacement field is therefore given by: $D = (D_{BG} - D_{TG})/2$. As mentioned before, in the absence of gating ($D = 0$), the conduction and valence bands of BLG touch one another with zero band gap. Upon electrical gating, the average electrical displacement field, $|D|$, breaks the inversion symmetry of BLG and generates a nonzero band gap.[5−12]

Using the defined electric displacement fields, the resistivities of BLG as a function of D_{BG} and D_{TG} for pristine, $I_D/I_G = 0.8$, and $I_D/I_G = 1.8$ devices are shown in Figure 5d−f, respectively. For each contour, we observe a rise of resistivity with $|D|$ along the diagonal, corresponding to the trajectory of CNPs, representing the signature behavior of a dual-gated BLG device.[5−12] The electronic transport in functionalized bilayer graphene still exhibits a strong dependence on the transverse electric displacement field, and the characteristics associated with the symmetry breaking at a high transverse electric displacement field are preserved. Quite surprisingly, we find that even the highest degree of functionalization considered ($I_D/I_G = 1.8$) does not undermine the lattice structure of AB-stacked BLG, so the symmetry breaking still dominates the transport in functionalized BLG. However, similar to the transport in functionalized MLG, because theoretically an ∼1 eV band gap can be created locally in the S-region due to the grafted functional groups on the top graphitic layer,[19] we expect that the quantum interference effect also plays an important role depending on the degree of functionalization. The formation of a transport band gap in a dual-gated, functionalized BLG device likely results from the effects of symmetry breaking and quantum interference.

To uncover the relation between the symmetry breaking and the quantum interference effects in functionalized BLG, the resistivities for the three BLG devices considered at $D_{BG} = 0$ and $D_{BG} = 1.4$ V/nm are plotted against D_{TG} in Figure 5g and h, respectively. A small degree of electron−hole conduction asymmetry was found in the pristine BLG device due to the n-type doping from the top-gate dielectrics.[56] At $D_{BG} = 0$ V/nm

(Figure 5g), the transport characteristics of functionalized BLG are similar to those of the bottom-gated MLG devices (see Figure 3a). The slow increase of R_{max} with I_D/I_G suggests that the electronic transport in functionalized BLG is also disorder-limited, although a band gap is created locally. However, under a positive electrical displacement field D_{BG} = 1.4 V/nm (Figure 5h), the R_{max} value increases significantly with I_D/I_G, and the on/off current ratio increases by 50%. The measured values of R_{max} along the trajectory of CNPs as a function of D for the three BLG devices considered here are shown in Figure 5i. In pristine BLG, R_{max} is almost symmetric with respect to $D = 0$;[10] however, a significant asymmetry is induced by the chemical functionalization. Interestingly, for $D < 0$, the three curves are almost parallel, while a drastic increase of R_{max} is observed at highly positive D and I_D/I_G. We believe that this implies the formation of a larger transport band gap due to the complicated interactions between the effects of chemical doping, disorder, symmetry breaking, and quantum interference. A future study will attempt to gain a better understanding of the electronic transport in this regime.

Conclusion. In conclusion, we have demonstrated an efficient method to covalently functionalize MLG and BLG in a precise and controllable manner using an electrochemical aryl diazonium chemistry. Using this method, for the first time, we have studied the transport characteristics of bottom-gated MLG and dual-gated BLG FET devices as a function of I_D/I_G, which provides insight on the electronic transport in functionalized graphene. We have shown that the electronic transport in functionalized graphene is limited by the formation of electron−hole puddles and midgap states due to chemical functionalization. The effective transport band gap is typically three orders of magnitude smaller than that predicted by the theory. A more significant transport band gap can be created in functionalized BLG at a highly positive transverse electric displacement field.

ASSOCIATED CONTENT

Supporting Information

Additional experimental details regarding device fabrication and characterization. This material is available free of charge via the Internet at http://pubs.acs.org.

AUTHOR INFORMATION

Corresponding Author

*E-mail: strano@mit.edu.

Notes

The authors declare no competing financial interest.

ACKNOWLEDGMENTS

M.S.S. acknowledges funding from the 2009 U.S. Office of Naval Research Multi University Research Initiative (ONR-MURI) on Graphene Advanced Terahertz Engineering (GATE) at MIT, Harvard and Boston University. M.S.S. is also grateful for a 2008 Young Investigator Program Award (YIP) from the U.S. Office of Naval Research. D.B. and M.S.S. are grateful for the financial support from the National Science Foundation CBET-1133813. C.J.S. is grateful for partial financial support from the Chyn Duog Shiah memorial Fellowship awarded by Massachusetts Institute of Technology. The authors thank J. Kong, A. Hsu, J. Sanchez-Yamagishi, T. Taychatanapat, and I. J. Wang for useful discussions and suggestions.

REFERENCES

(1) Geim, A. K.; Novoselov, K. S. *Nat. Mater.* **2007**, *6* (3), 183−191.
(2) Chen, J. H.; Jang, C.; Xiao, S. D.; Ishigami, M.; Fuhrer, M. S. *Nat. Nanotechnol.* **2008**, *3* (4), 206−209.
(3) Bolotin, K. I.; Sikes, K. J.; Jiang, Z.; Klima, M.; Fudenberg, G.; Hone, J.; Kim, P.; Stormer, H. L. *Solid State Commun.* **2008**, *146* (9−10), 351−355.
(4) Dean, C. R.; Young, A. F.; Meric, I.; Lee, C.; Wang, L.; Sorgenfrei, S.; Watanabe, K.; Taniguchi, T.; Kim, P.; Shepard, K. L.; Hone, J. *Nat. Nanotechnol.* **2010**, *5* (10), 722−726.
(5) Ohta, T.; Bostwick, A.; Seyller, T.; Horn, K.; Rotenberg, E. *Science* **2006**, *313* (5789), 951−954.
(6) Oostinga, J. B.; Heersche, H. B.; Liu, X. L.; Morpurgo, A. F.; Vandersypen, L. M. K. *Nat. Mater.* **2008**, *7* (2), 151−157.
(7) Xia, F. N.; Farmer, D. B.; Lin, Y. M.; Avouris, P. *Nano Lett.* **2010**, *10* (2), 715−718.
(8) Zhang, Y. B.; Tang, T. T.; Girit, C.; Hao, Z.; Martin, M. C.; Zettl, A.; Crommie, M. F.; Shen, Y. R.; Wang, F. *Nature* **2009**, *459* (7248), 820−823.
(9) Mak, K. F.; Lui, C. H.; Shan, J.; Heinz, T. F. *Phys. Rev. Lett.* **2009**, *102* (25), 256405.
(10) Taychatanapat, T.; Jarillo-Herrero, P. *Phys. Rev. Lett.* **2010**, *105* (16), 166601.
(11) Miyazaki, H.; Tsukagoshi, K.; Kanda, A.; Otani, M.; Okada, S. *Nano Lett.* **2010**, *10* (10), 3888−3892.
(12) Yan, J.; Kim, M. H.; Elle, J. A.; Sushkov, A. B.; Jenkins, G. S.; Milchberg, H. M.; Fuhrer, M. S.; Drew, H. D. *Nat. Nanotechnol.* **2012**, *7* (7), 472−478.
(13) Son, Y. W.; Cohen, M. L.; Louie, S. G. *Phys. Rev. Lett.* **2006**, *97* (21), 216803.
(14) Chen, Z. H.; Lin, Y. M.; Rooks, M. J.; Avouris, P. *Physica E* **2007**, *40* (2), 228−232.
(15) Han, M. Y.; Ozyilmaz, B.; Zhang, Y. B.; Kim, P. *Phys. Rev. Lett.* **2007**, *98* (20), 206805.
(16) Bai, J. W.; Zhong, X.; Jiang, S.; Huang, Y.; Duan, X. F. *Nat. Nanotechnol.* **2010**, *5* (3), 190−194.
(17) Pereira, V. M.; Neto, A. H. C. *Phys. Rev. Lett.* **2009**, *103* (4), 046801.
(18) Bao, W. Z.; Miao, F.; Chen, Z.; Zhang, H.; Jang, W. Y.; Dames, C.; Lau, C. N. *Nat. Nanotechnol.* **2009**, *4* (9), 562−566.
(19) Boukhvalov, D. W.; Katsnelson, M. I. *Phys. Rev. B* **2008**, *78* (8), 085413.
(20) Ryu, S.; Han, M. Y.; Maultzsch, J.; Heinz, T. F.; Kim, P.; Steigerwald, M. L.; Brus, L. E. *Nano Lett.* **2008**, *8* (12), 4597−4602.
(21) Elias, D. C.; Nair, R. R.; Mohiuddin, T. M. G.; Morozov, S. V.; Blake, P.; Halsall, M. P.; Ferrari, A. C.; Boukhvalov, D. W.; Katsnelson, M. I.; Geim, A. K.; Novoselov, K. S. *Science* **2009**, *323* (5914), 610−613.
(22) Cheng, S. H.; Zou, K.; Okino, F.; Gutierrez, H. R.; Gupta, A.; Shen, N.; Eklund, P. C.; Sofo, J. O.; Zhu, J. *Phys. Rev. B* **2010**, *81* (20), 205435.
(23) Sarkar, S.; Bekyarova, E.; Haddon, R. C. *Acc. Chem. Res.* **2012**, *45* (4), 673−682.
(24) Niyogi, S.; Bekyarova, E.; Hong, J.; Khizroev, S.; Berger, C.; de Heer, W.; Haddon, R. C. *J. Phys. Chem. Lett.* **2011**, *2* (19), 2487−2498.
(25) Haberer, D.; Vyalikh, D. V.; Taioli, S.; Dora, B.; Farjam, M.; Fink, J.; Marchenko, D.; Pichler, T.; Ziegler, K.; Simonucci, S.; Dresselhaus, M. S.; Knupfer, M.; Buchner, B.; Gruneis, A. *Nano Lett.* **2010**, *10* (9), 3360−3366.
(26) Dikin, D. A.; Stankovich, S.; Zimney, E. J.; Piner, R. D.; Dommett, G. H. B.; Evmenenko, G.; Nguyen, S. T.; Ruoff, R. S. *Nature* **2007**, *448* (7152), 457−460.
(27) Moser, J.; Tao, H.; Roche, S.; Alzina, F.; Torres, C. M. S.; Bachtold, A. *Phys. Rev. B* **2010**, *81* (20), 205445.
(28) Wang, S. N.; Wang, R.; Liu, X. F.; Wang, X. W.; Zhang, D. D.; Guo, Y. J.; Qiu, X. H. *J. Phys. Chem. C* **2012**, *116* (19), 10702−10707.
(29) Withers, F.; Dubois, M.; Savchenko, A. K. *Phys. Rev. B* **2010**, *82* (7), 073403.

(30) Nair, R. R.; Ren, W. C.; Jalil, R.; Riaz, I.; Kravets, V. G.; Britnell, L.; Blake, P.; Schedin, F.; Mayorov, A. S.; Yuan, S. J.; Katsnelson, M. I.; Cheng, H. M.; Strupinski, W.; Bulusheva, L. G.; Okotrub, A. V.; Grigorieva, I. V.; Grigorenko, A. N.; Novoselov, K. S.; Geim, A. K. *Small* **2010**, *6* (24), 2877−2884.
(31) Withers, F.; Bointon, T. H.; Dubois, M.; Russo, S.; Craciun, M. F. *Nano Lett.* **2011**, *11* (9), 3912−3916.
(32) Bekyarova, E.; Itkis, M. E.; Ramesh, P.; Berger, C.; Sprinkle, M.; de Heer, W. A.; Haddon, R. C. *J. Am. Chem. Soc.* **2009**, *131* (4), 1336−1337.
(33) Niyogi, S.; Bekyarova, E.; Itkis, M. E.; Zhang, H.; Shepperd, K.; Hicks, J.; Sprinkle, M.; Berger, C.; Lau, C. N.; Deheer, W. A.; Conrad, E. H.; Haddon, R. C. *Nano Lett.* **2010**, *10* (10), 4061−4066.
(34) Sharma, R.; Baik, J. H.; Perera, C. J.; Strano, M. S. *Nano Lett.* **2010**, *10* (2), 398−405.
(35) Zhang, H.; Bekyarova, E.; Huang, J. W.; Zhao, Z.; Bao, W. Z.; Wang, F. L.; Haddon, R. C.; Lau, C. N. *Nano Lett.* **2011**, *11* (10), 4047−4051.
(36) Koehler, F. M.; Jacobsen, A.; Ensslin, K.; Stampfer, C.; Stark, W. J. *Small* **2010**, *6* (10), 1125−1130.
(37) Sinitskii, A.; Dimiev, A.; Corley, D. A.; Fursina, A. A.; Kosynkin, D. V.; Tour, J. M. *ACS Nano* **2010**, *4* (4), 1949−1954.
(38) Fan, X. Y.; Nouchi, R.; Yin, L. C.; Tanigaki, K. *Nanotechnology* **2010**, *21* (47), 475208.
(39) Paulus, G. L. C.; Wang, Q. H.; Strano, M. S. *Acc. Chem. Res.* **2012**, DOI: 10.1021/ar300119z.
(40) Fan, X. Y.; Nouchi, R.; Tanigaki, K. *J. Phys. Chem. C* **2011**, *115* (26), 12960−12964.
(41) Wang, Q. H.; Jin, Z.; Kim, K. K.; Hilmer, A. J.; Paulus, G. L. C.; Shih, C. J.; Ham, M. H.; Sanchez-Yamagishi; Watanabe, K.; Taniguchi, T.; Kong, J.; Jarillo-Herrero, P.; Strano, M. S. *Nat. Chem.* **2012**, *4*, 724−732.
(42) Suzuura, H.; Ando, T. *Phys. Rev. Lett.* **2002**, *89* (26), 266603.
(43) Lucchese, M. M.; Stavale, F.; Ferreira, E. H. M.; Vilani, C.; Moutinho, M. V. O.; Capaz, R. B.; Achete, C. A.; Jorio, A. *Carbon* **2010**, *48* (5), 1592−1597.
(44) Israelachvili, J. N. *Intermolecular and surface forces*, 3rd ed.; Academic Press: Burlington, MA, 2011.
(45) Das, A.; Pisana, S.; Chakraborty, B.; Piscanec, S.; Saha, S. K.; Waghmare, U. V.; Novoselov, K. S.; Krishnamurthy, H. R.; Geim, A. K.; Ferrari, A. C.; Sood, A. K. *Nat. Nanotechnol.* **2008**, *3* (4), 210−215.
(46) Wang, Q. H.; Hersam, M. C. *Nat. Chem.* **2009**, *1* (3), 206−211.
(47) Farmer, D. B.; Golizadeh-Mojarad, R.; Perebeinos, V.; Lin, Y. M.; Tulevski, G. S.; Tsang, J. C.; Avouris, P. *Nano Lett.* **2009**, *9* (1), 388−392.
(48) Ferrari, A. C.; Meyer, J. C.; Scardaci, V.; Casiraghi, C.; Lazzeri, M.; Mauri, F.; Piscanec, S.; Jiang, D.; Novoselov, K. S.; Roth, S.; Geim, A. K. *Phys. Rev. Lett.* **2006**, *97* (18), 187401.
(49) Ferreira, E. H. M.; Moutinho, M. V. O.; Stavale, F.; Lucchese, M. M.; Capaz, R. B.; Achete, C. A.; Jorio, A. *Phys. Rev. B* **2010**, *82* (12), 125429.
(50) Malard, L. M.; Pimenta, M. A.; Dresselhaus, G.; Dresselhaus, M. S. *Phys. Rep.* **2009**, *473* (5−6), 51−87.
(51) Das, A.; Chakraborty, B.; Piscanec, S.; Pisana, S.; Sood, A. K.; Ferrari, A. C. *Phys. Rev. B* **2009**, *79*, 15.
(52) Zhang, Z. M. *Nano/microscale heat transfer*; McGraw-Hill: New York, NY, 2007.
(53) Adam, S.; Hwang, E. H.; Galitski, V. M.; Das Sarma, S. *Proc. Natl. Acad. Sci. U.S.A.* **2007**, *104* (47), 18392−18397.
(54) Shih, C. J.; Paulus, G. L. C.; Wang, Q. H.; Jin, Z.; Blankschtein, D.; Strano, M. S. *Langmuir* **2012**, *28* (22), 8579−8586.
(55) Wehling, T. O.; Yuan, S.; Lichtenstein, A. I.; Geim, A. K.; Katsnelson, M. I. *Phys. Rev. Lett.* **2010**, *105* (5), 056802.
(56) Fu, W. Y.; Nef, C.; Knopfrnacher, O.; Tarasov, A.; Weiss, M.; Calame, M.; Schonenberger, C. *Nano Lett.* **2011**, *11* (9), 3597−3600.